Integrin-mediated adhesion regulates membrane order

Katharina Gaus,[1,2] Soazig Le Lay,[3] Nagaraj Balasubramanian,[4] and Martin A. Schwartz[4,5,6]

[1]Centre for Vascular Research, School of Medical Sciences, University of New South Wales, Sydney, 2052 NSW, Australia
[2]Department of Haematology, Prince of Wales Hospital, Sydney, 2052 NSW, Australia
[3]Max Planck Institute for Molecular Cell Biology and Genetics, 01307 Dresden, Germany
[4]Cardiovascular Research Center, [5]Department of Microbiology, and [6]Department of Biomedical Engineering, University of Virginia, Charlottesville, VA 22936

The properties of cholesterol-dependent domains (lipid rafts) in cell membranes have been controversial. Because integrin-mediated cell adhesion and caveolin both regulate trafficking of raft components, we investigated the effects of adhesion and caveolin on membrane order. The fluorescent probe Laurdan and two-photon microscopy revealed that focal adhesions are highly ordered; in fact, they are more ordered than caveolae or domains that stain with cholera toxin subunit B (CtxB). Membrane order at focal adhesion depends partly on phosphorylation of caveolin1 at Tyr14, which localizes to focal adhesions. Detachment of cells from the substratum triggers a rapid, caveolin-independent decrease in membrane order, followed by a slower, caveolin-dependent decrease that correlates with internalization of CtxB-stained domains. Endocytosed CtxB domains also become more fluid. Thus, membrane order is highly dependent on caveolae and focal adhesions. These results show that lipid raft properties are conferred by assembly of specific protein complexes. The ordered state within focal adhesions may have important consequences for signaling at these sites.

Introduction

Eukaryotic plasma membranes are thought to contain dynamic microdomains called lipid rafts, which are proposed to be cholesterol- and sphingolipid-rich ordered domains that "float" in an environment of more fluid regions (Simons and Toomre, 2000; Kusumi et al., 2004). However, some authors have argued that rafts are not preexisting structures in cell membranes, but are induced by clustering of raft components (Harris and Siu, 2002). It has also been suggested that rafts may simply be artifactual (Munro, 2003). Rafts were initially defined by their insolubility in the detergent Triton X-100 (Brown and London, 1998). Many proteins, including important signaling molecules, preferentially partition into these fractions (Simons and Ikonen, 1997). However, because cold detergents can scramble lipids (Heerklotz et al., 2003; Gaus et al., 2005b), these membranes cannot be equated with native microdomains (Munro, 2003). In cells, glycosyl-phosphatidylinositol–anchored and myristoylated/palmitoylated proteins have been reported to be present in cholesterol-dependent domains that are tens of nanometers in diameter (Varma and Mayor, 1998; Zacharias et al., 2002; Sharma et al., 2004). In addition, caveolae represent a subtype of lipid raft that form flask-shaped membrane invaginations containing the structural protein caveolin1 (Cav1; Pelkmans and Zerial, 2005). Cav1 directly interacts with cholesterol, palmitic acid, and stearic acid and has been implicated in signal transduction (Razani et al., 2002) and endocytosis (Pelkmans and Helenius, 2002), particularly of cholera toxin subunit B (CtxB), which binds to the ganglioside GM1 (Pelkmans et al., 2002).

Cell adhesion to the ECM is mediated mainly by integrins, which, when in culture, cluster with numerous cytoskeletal and signaling proteins at focal adhesions and focal complexes (Schwartz, 1997). Integrins control many signaling events that are critical for cell survival, growth, and gene expression (Schwartz, 2001; Hynes, 2002). Both integrin clustering and changes in conformation caused by ligand binding contribute to these signaling events. Additionally, integrin binding to ECM proteins is controlled by intracellular signaling pathways. There are several reports linking integrins with lipid rafts and/or caveolin. Functional activation of integrins, i.e., conversion to the high affinity state, appears to be linked to lipid raft localization (Porter and Hogg, 1998; Chapman et al., 1999; Wei et al., 1999; Decker and Ffrench-Constant, 2004). Caveolin was reported to physically associate with integrins (Wary et al., 1998;

Correspondence to Katharina Gaus: k.gaus@unsw.edu.au; or Martin Schwartz: maschwartz@virginia.edu

Abbreviations used in this paper: CtxB, cholera toxin subunit B; GP, general polarization; mβCD, methyl-β-cyclodextrin; MEF, mouse embryonic fibroblast; PAEC, pig aortic endothelial cells; TfR, transferrin receptor; WT, wild type.

The online version of this article contains supplemental material.

The Journal of Cell Biology, Vol. 174, No. 5, August 28, 2006 725–734
http://www.jcb.org/cgi/doi/10.1083/jcb.200603034

Chapman et al., 1999; Wei et al., 1999). Recently, it was shown that integrin-mediated adhesion regulates the trafficking of lipid raft components such that when cells are detached multiple raft markers are rapidly internalized (del Pozo et al., 2004). This process requires dynamin2 and caveolin1 phosphorylated at Tyr 14 (del Pozo et al., 2005). The phosphorylated caveolin1 (pYCav1) localizes to focal adhesions in adherent cells, but relocalizes to caveolae when cells are detached.

We analyzed membrane order at focal adhesions and determined its dependence on integrins, Cav1 expression, and phosphorylation. We used the membrane dye Laurdan in conjunction with two-photon laser scanning microscopy, which has been used extensively to define ordered domains in artificial membranes (Bagatolli et al., 2003) and in live and fixed cells (Gaus et al., 2003). In macrophages, neutrophils, and activated T lymphocytes, condensed membranes cover a significant proportion of the cell surface and are frequently associated with actin-rich membrane protrusions (Gaus et al., 2003; Kindzelskii et al., 2004) or immunological synapses (Gaus et al., 2005a). Our results show that membrane order is highly dependent on integrin binding to the ECM, that focal adhesions are sites of high membrane order, and that these events are partially dependent on caveolin.

Results

Membrane lipids in focal adhesions are highly ordered

To assess the physical state of cell membranes, we analyzed Laurdan fluorescence using two-photon microscopy. The Laurdan probe does not preferentially partition into either lipid phase, but aligns parallel to the phospholipids (Bagatolli et al., 2003) and undergoes a shift in its peak emission wavelength from ~500 nm in fluid membranes to ~440 nm in ordered membranes. The shift to longer emission wavelength is caused by partial penetration of water molecules into more fluid membranes; a polar environment favors an internal charge transfer state of the probe with an energetically lower excited state and, hence, a longer emission wavelength (Gaus et al., 2006). A normalized ratio of the two emission regions, given by the general polarization (GP), provides a relative measure of membrane order. GP values are, in principle, between –1 and +1, with fluid domains ranging from ~0.05 to 0.25 and ordered domains ranging from 0.25 to 0.55 (Gaus et al., 2006). Although Laurdan has reported different lipid phases in liposomes (Bagatolli et al., 2003), phase separation in cell plasma membranes has not been observed (Gaus et al., 2003). In the complex environment of cell membranes, GP values reflect the overall membrane structure. When cells are fixed and immunolabeled, Laurdan does not bind to or become trapped in complexes or membrane domains, as indicated by complete extraction by 0.1% Triton X-100 (Fig. S1 A, available at http://www.jcb.org/cgi/content/full/jcb.200603034/DC1). However, we cannot completely exclude that proteins, or perhaps physical parameters of membranes other than lipid packing, could affect Laurdan's spectral properties.

Serum-starved pig aortic endothelial cells (PAEC) on fibronectin (FN)-coated glass coverslips were imaged at the basal membrane. GP images (Fig. 1, A, F, and K) show punctuated,

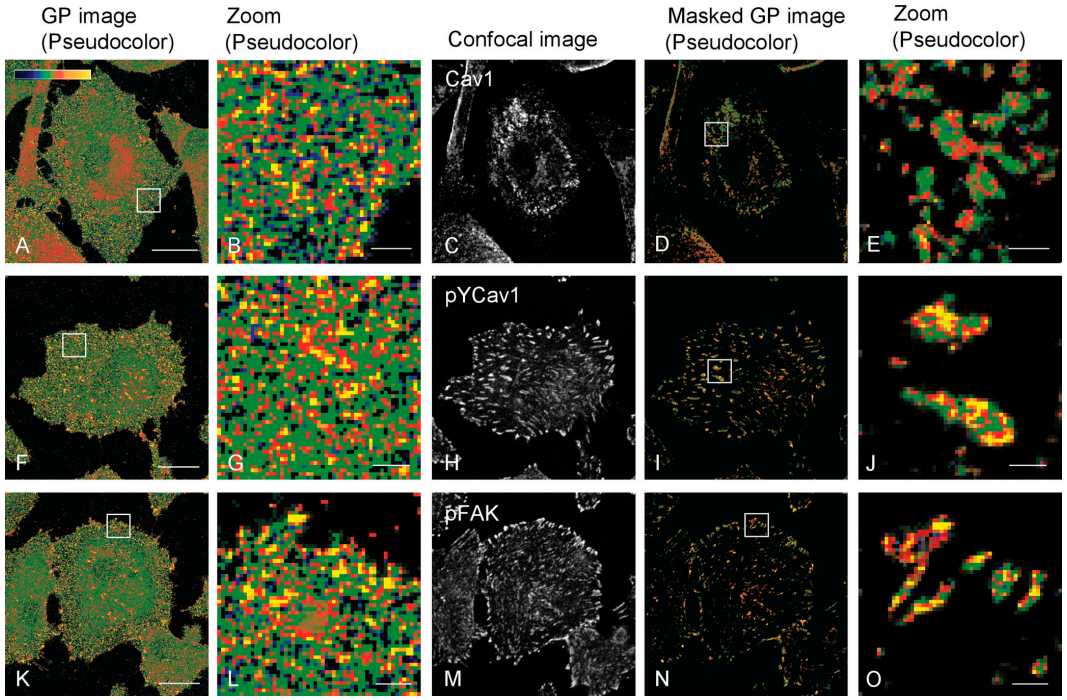

Figure 1. **GP and immunofluorescence images of PAEC.** PAEC on FN-coated glass coverslips for 2–4 h were Laurdan labeled, fixed, and immunostained as described in Materials and methods. GP images (A, F, and K) were calculated from intensity images (see Materials and methods) and pseudocolored with blue to yellow representing low to high GP values, respectively (see color scale in A). B, G, and L show magnified regions of the GP images. Image in C is stained for Cav1, in H is stained for pYCav1, and in M for pFAK. In D, I, and N, GP values are shown only for the pixels where immunostains are above background. E, J, and O show magnified regions of the masked GP images. Bars: (A, F, and K) 20 μm; (B, G, L, E, J, and O) 2 μm.

Table I. **GP values of immunostained adherent or detached PAECs**

Marker	PAEC adherent	PAEC detached
Cav1[1]	0.392 ± 0.072 (n = 31)[a]	0.383 ± 0.059 (n = 18)
pYCav1[1]	0.482 ± 0.075 (n = 28)[a,b]	0.419 ± 0.053 (n = 20)[b]
pFAK	0.502 ± 0.067 (n = 33)	N/A
CTxB[1]	0.430 ± 0.084 (n = 12)	0.388 ± 0.054 (n = 16)[c,d]
CTxB (15 min)		0.350 ± 0.056 (n = 13)
CTxB (30 min)		0.283 ± 0.056 (n = 12)[c]
CTxB (120 min)		0.243 ± 0.054 (n = 12)[d]

Adherent or detached PAECs were labeled with Laurdan and other markers and imaged as described in Materials and methods. GP images and confocal images at identical focal planes were compared pixel by pixel to determine the mean GP value ± SD (from n images) within pixels positively stained for Cav1, pYCav1, pFAK, and CTxB as indicated in Fig. 1. Pairs of superscripts indicate statistically significant differences between the two values sharing the same superscript.
[1]1–2 min in suspension if detached.
[a,b]$P < 0.05$.
[c,d]$P < 0.001$. Note that no significant differences were found in mean GP value of Cav1- or CTxB-stained membranes between adherent and detached cells.

irregularly distributed, high GP domains pseudocolored yellow to red. Shown at a higher magnification in Fig. 1 (B, G, and L), these ordered domains are typically a few pixels in diameter, where a single pixel (~215 × 215 nm) is close to the spatial resolution of the microscope (183 nm). The high GP domains seen in adherent PAEC are therefore 0.2–1.0 μm in diameter. It is important to note that these areas do not necessarily represent single membrane domains, but rather areas in which the fraction of ordered domains is higher.

To identify distinct membrane structures, we immunolabeled these cells with antibodies against phosphorylated FAK (pFAK) and phosphorylated caveolin-1 (pYCav1) as focal adhesion markers (del Pozo et al., 2005), total Cav1 as a caveolar marker, or Cy3-conjugated CTxB, which binds to GM1 and is a well-established marker for lipid rafts (Fra et al., 1994). To correlate GP with focal adhesions, we used the immunofluorescent images to mask the GP images; the masked GP images only show the immunostained pixels, using the same pseudocoloring to indicate GP values. Fig. 1 (D, I, and N) shows the masked GP images of Cav1, pYCav1, and pFAK, respectively. Particularly when magnified (Fig. 1, E, J, and O), it becomes apparent that pYCav1- and pFAK-stained pixels are substantially enriched in high GP areas colored yellow and red, whereas Cav1-stained pixels select GP values at the border between red and green. Even within a focal adhesion, GP values are not homogenous, indicating the absence of phase boundaries, as well as the complexity of these membrane sites.

To quantify GP values within the immunoselected areas, we determined the average GP values of the masked images and calculated the mean of n images. This pixel-per-pixel comparison gives a "fluidity" index for pixels that stain positively for selected markers. Table I clearly shows that pFAK-positive regions are highly ordered, with a mean GP value (0.502 ± 0.067) that is even higher than CTxB-stained areas (0.430 ± 0.084). In contrast, GP values averaged over the entire cell are 0.23 (Fig. 2). As a control, we determined the GP value of transferrin receptor (TfR)–stained regions (Fig. S1; 0.165 ± 0.066), which was consistent with the exclusion of TfR from cholesterol-rich domains (Harder et al., 1998). Triggering TfR uptake resulted in a similar mean GP value, suggesting that neither surface-bound TfR nor coated pits or endosomes contain a high fraction of ordered domains. Collectively, these results show that focal adhesions are highly ordered.

It has been shown previously that Cav1 phosphorylated on Y14 localizes to focal adhesions (Scherer et al., 1997; Wary et al., 1998; del Pozo et al., 2005). This phosphorylated fraction comprises <1% of the total Cav1 (del Pozo et al., 2005); thus, the total Cav1 staining of focal adhesions is very weak. Cav1 instead localizes to distinct regions of the cell (Fig. 1 C), where, presumably, caveolae are abundant. Overlaying GP with images of Cav1 or pYCav1 showed that these regions are also highly ordered (Fig. 1, E and J, and Table I). Interestingly, GP was higher in pixels positive for pYCav1 than for Cav1 ($P < 0.05$), which is consistent with focal adhesions being very highly ordered.

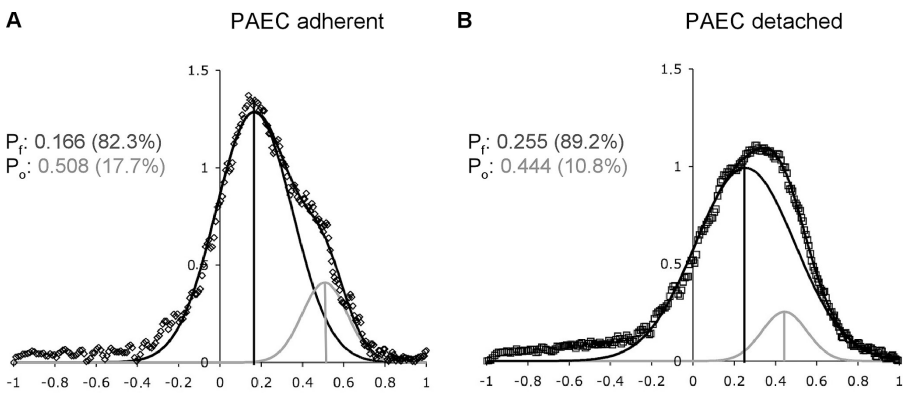

Figure 2. **Global GP distributions of adherent and detached PAEC.** PAEC were plated on FN-coated coverslips for 2–4 h (A, open diamonds) or suspended for ~1–2 min (B, open squares). GP images ($n > 12$), from a single experiment to minimize differences in Laurdan distribution between intracellular membranes, were recorded close to the coverslip, normalized, and fitted to two Gaussian populations (line through data). Black vertical lines denote the centers of the fluid population (P_f); gray vertical lines denote the centers of the ordered populations (P_o). Center values and coverages are given for both populations. ERFs, which quantifies the quality of the fit to the data (see Materials and methods), are 0.0071 and 0.0062 for A and B, respectively.

We next determined whether membrane structure at pYCav1-stained regions depends on cholesterol (Fig. S2, available at http://www.jcb.org/cgi/content/full/jcb.200603034/DC1). After cholesterol depletion with 10 mM methyl-β-cyclodextrin (mβCD) for 1 h, the mean GP value at these regions decreased to 0.293 ± 0.077 (n = 19; P < 0.001). The mean GP value was restored to 0.508 ± 0.049 (n = 17) after cholesterol-depleted cells were incubated with 15 μg/ml cholesterol complexed to 0.37 mM mβCD for an additional 1 h. These data indicate that membrane order at focal adhesions depends on cholesterol.

Effects of cell adhesion

The localization of CtxB to Cav1-enriched domains increased 2–10 min after the detachment of cells from the substratum and was followed by internalization of the CtxB (del Pozo et al., 2005). Therefore, we analyzed the effects of cell adhesion on membrane structure. After detachment, all membrane domains become more fluid (Table I); CtxB-positive domains in particular showed a drastic, time-dependent decrease in mean GP. However, a difference in mean GP after 1–2 min of detachment was only significant for the focal adhesion marker pYCav1, suggesting that the structure of pYCav1-containing membrane domains is dependent on integrin engagement. It is also noteworthy that Cav1 and pYCav1 are located in membrane domains of similar GP value in detached cells, whereas pYCav1 was found in more ordered domains in adherent cells. This observation is consistent with increased colocalization of pYCav1 with Cav1 upon detachment (del Pozo et al., 2005). Collectively, the data suggest that membrane order at focal adhesions is higher than that at caveolae, and that focal adhesion, but not caveolar membrane structure, is dependent on integrin engagement.

Keeping endothelial cells in suspension triggers the internalization of GM1-containing membrane domains (unpublished data), just as in fibroblasts (del Pozo et al., 2004). Consistent with this result, the mean GP of internalized GM1-containing raft membranes showed a statistically significant, time-dependent decrease after detachment (Table I). This finding is in agreement with the increased solubility of GM1 in cold detergent after cell detachment (del Pozo et al., 2005). Collectively, the data suggest that not only are ordered domains internalized when cells are detached but also that membrane organization is drastically perturbed as a result of this process.

Fig. 2 compares the global membrane structure of adherent PAEC with PAEC suspended for 1–2 min. Normalized GP histograms can be accurately described by fitting to two Gaussian populations (error function [ERF] < 0.01). In adherent cells, the fluid population covered 82.3% of the surface and the mean GP was 0.166; ordered domains covered 17.7% and mean GP was 0.508. Immediately after detachment, the GP of the ordered population decreased to 0.444, while its abundance decreased to 10.8%. It is interesting to note that the fluid population increased its coverage to 89.2%, but became more ordered (mean GP 0.255). This result suggests that components that confer order, such as cholesterol, may have moved from the rafts into the bulk membrane.

Membrane order of focal adhesion is partly dependent on Cav1 expression

To investigate whether the high degree of order within focal adhesions requires Cav1, we examined mouse embryonic fibroblasts (MEFs) from wild-type (WT) and Cav1$^{-/-}$ animals. Distribution of pFAK in MEFs on FN was similar in both cell types (Fig. 3, B and F), demonstrating that focal adhesions are not compromised in Cav1$^{-/-}$ cells, as previously reported (del Pozo et al., 2005). However, analysis of GP revealed that focal adhesions were significantly more ordered in WT MEFs compared with Cav1$^{-/-}$ MEFs (Table II and Fig. 3, D and H), although lower than those in PAEC. We next compared CtxB-enriched domains in both cell types. The intensity of CTxB staining was similar in both cell types (unpublished data) and a comparison of GP values in CTxB-positive pixels revealed no significant difference between Cav1$^{-/-}$ and WT MEFs (Table II).

Previous work suggested that lipid rafts may influence integrin function, with integrin activation, clustering, and adhesion being raft-dependent (Leitinger and Hogg, 2002). Therefore, we considered that integrin affinities may be lower in Cav1$^{-/-}$ compared with WT cells, which in turn could influence membrane order at focal adhesions. Affinity state for integrin α5β1, which is the main FN receptor, was measured by the binding of a soluble integrin-binding fragment of FN that has

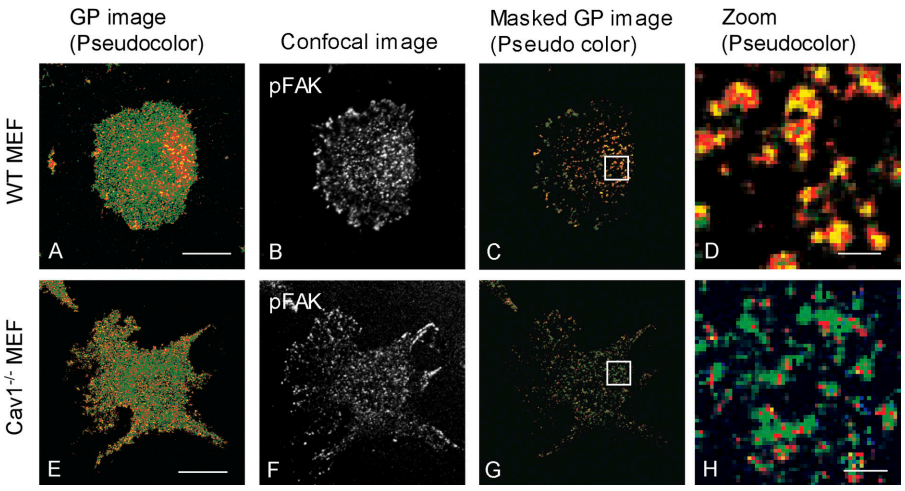

Figure 3. **GP and immunofluorescent images of WT and Cav1$^{-/-}$ MEFs.** WT (A–D) and Cav1$^{-/-}$ (E–H) MEFs on FN-coated glass coverslips for 2–4 h were Laurdan labeled, immunostained, and imaged as described in Materials and methods. GP image pseudocoloring (A and E) and masking with confocal images were performed as for Fig. 1. B and F show the corresponding confocal images of pFAK, C and G show GP values of pFAK-stained pixels, and D and H show magnified sections of the masked GP images. Bars: (A and E) 20 μm; (D and H) 2 μm.

Table II. **GP values of immunostained adherent or detached MEFs**

Adherent MEFs	WT MEFs	Cav1$^{-/-}$ MEFs
Cav1	0.382 ± 0.070 (n = 27)[a]	
pYCav1	0.459 ± 0.076 (n = 24)[a]	
pFAK	0.422 ± 0.058 (n = 24)[b]	0.297 ± 0.080 (n = 28)[b]
CTxB	0.434 ± 0.069 (n = 11)	0.442 ± 0.099 (n = 10)
Detached MEFs		
CTxB (1 min)	0.368 ± 0.061 (n = 13)[α,β]	0.370 ± 0.032 (n = 12)
CTxB (15 min)	0.306 ± 0.060 (n = 12)[c]	0.365 ± 0.050 (n = 12)[c]
CTxB (30 min)	0.270 ± 0.058 (n = 16)[d,α]	0.353 ± 0.040 (n = 12)[d]
CTxB (120 min)	0.212 ± 0.086 (n = 14)[e,β]	0.330 ± 0.037 (n = 12)[e]

MEFs on FN-coated coverslip for 4 h (adherent) or in suspension for 1–120 min (detached) were labeled and imaged as described in Materials and methods. Mean GP values ± the SD (from n images) were calculated for pixels stained positively for Cav1, pYCav1, pFAK, and CTxB. Pairs of footnotes denote statistically significant differences between the two values sharing the same footnote.
[a,b]$P < 0.001$.
[c]$P < 0.05$.
[d,e]$P < 0.001$. c–e compare WT MEFs to Cav1$^{-/-}$ MEFs.
[α]$P < 0.05$.
[β]$P < 0.001$. α and β compare the kinetics of CTxB-labeled domains in WT MEFs. No significant differences were found between adherent cells and cells immediately after detachment (1 min) for both WT and Cav1$^{-/-}$ MEFs, and no differences were found in the kinetics of CTxB-labeled domains in Cav1$^{-/-}$ MEFs.

been used previously to measure α5β1 affinity (Faull et al., 1993). These measurements showed no difference between WT and Cav1$^{-/-}$ cells (Fig. S3, available at http://www.jcb.org/cgi/content/full/jcb.200603034/DC1). Integrin αvβ3 activation state, assayed by binding of the Fab fragment WOW1 (Pampori et al., 1999), also showed no difference (unpublished data). Thus, effects of caveolin on membrane order are not caused by changes in integrin affinity state.

Next, we compared the global GP distribution in adherent WT and Cav1$^{-/-}$ MEFs (Fig. 4). In WT MEFs, two populations were evident, one with mean GP = 0.178 and 71.4% coverage, and a second with GP = 0.565 and 28.6% coverage. In Cav1$^{-/-}$ MEFs, the fluid population had a mean GP of 0.161 and 91.9% coverage, while the ordered population had mean GP of 0.471 and 8.1% coverage. Hence, ordered domains in adherent Cav1$^{-/-}$ MEFs are both less abundant and less ordered. This difference is most likely caused by the combination of less-ordered focal adhesions and loss of caveolae. It should also be noted that Cav1$^{-/-}$ MEFs are enriched in cholesterol esters but depleted of unesterified cholesterol compared with WT MEFs (Frank et al., 2006), whereas the levels of major phospholipid classes are unaltered (unpublished data). These results are consistent with the known mechanism for autoregulation of cholesterol levels through SREBP cleavage (Horton, 2002). Changes in cholesterol levels and distribution could also contribute to the observed difference in GP distribution. Nevertheless, membranes outside of focal adhesions and caveolae were not significantly different, suggesting that these effects are specific.

Dependence of focal adhesion membrane structure on pYCav1

These results led us to ask whether changes in focal adhesion order in Cav1$^{-/-}$ cells are caused by global changes in membrane structure or by specific loss of pYCav1. Therefore, Cav1$^{-/-}$ MEFs were transfected either with FLAG-tagged WT Cav1 (Fig. 5, A–D) or FLAG-tagged Y14F Cav1 mutant (Fig. 5, E–H). WT and Y14F Cav1 expression levels were similar (not depicted), as were their staining patterns (Fig. 5, B and F). Flag-positive pixels had similar order (GP = 0.354 ± 0.057 for Y14F Cav1 and GP = 0.358 ± 0.060 for WT Cav1; see FLAG in Fig. 5 J), which matched caveolin-positive pixels in nontransfected WT MEF (GP = 0.382 ± 0.070; Table II) or mock-transfected WT MEFs (GP = 0.376 ± 0.042; Table S1, available at http://www.jcb.org/cgi/content/full/jcb.200603034/DC1). These results are consistent with the finding that Y14F Cav1 forms caveolae (del Pozo et al., 2005). Global GP histograms showed that both WT and Y14F Cav1 (Fig. 5 I) increased membrane order relative to nontransfected or mock-transfected Cav1$^{-/-}$ MEFs (Fig. 4 B and Table S1, respectively). However, WT Cav1 increased order to a greater extent (mean GP of ordered domains 0.535 vs. 0.487 in WT Cav1 vs. Y14F Cav1, respectively; Fig. 5 I) and coverage of ordered domains was higher

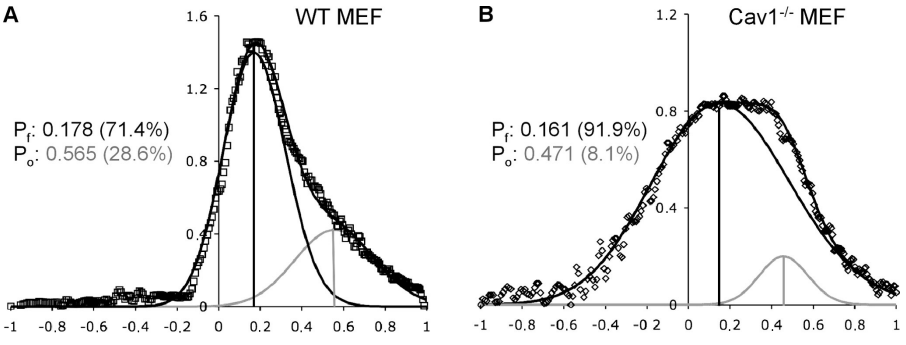

Figure 4. **Global GP distribution of adherent WT and Cav1$^{-/-}$ MEFs.** Normalized histograms for GP from Cav1$^{-/-}$ and WT MEFs on FN-coated coverslips (n >12 images from a single experiment) were fitted to two Gaussian populations (line through data). (A) WT MEFs (open diamonds). (B) Cav1$^{-/-}$ MEFs (open squares). Black vertical lines denote centers of the fluid, gray vertical lines of the ordered populations. Centers and coverages of fluid (P_f) and ordered (P_o) are given. ERF for A and B are 0.0086 and 0.0042, respectively.

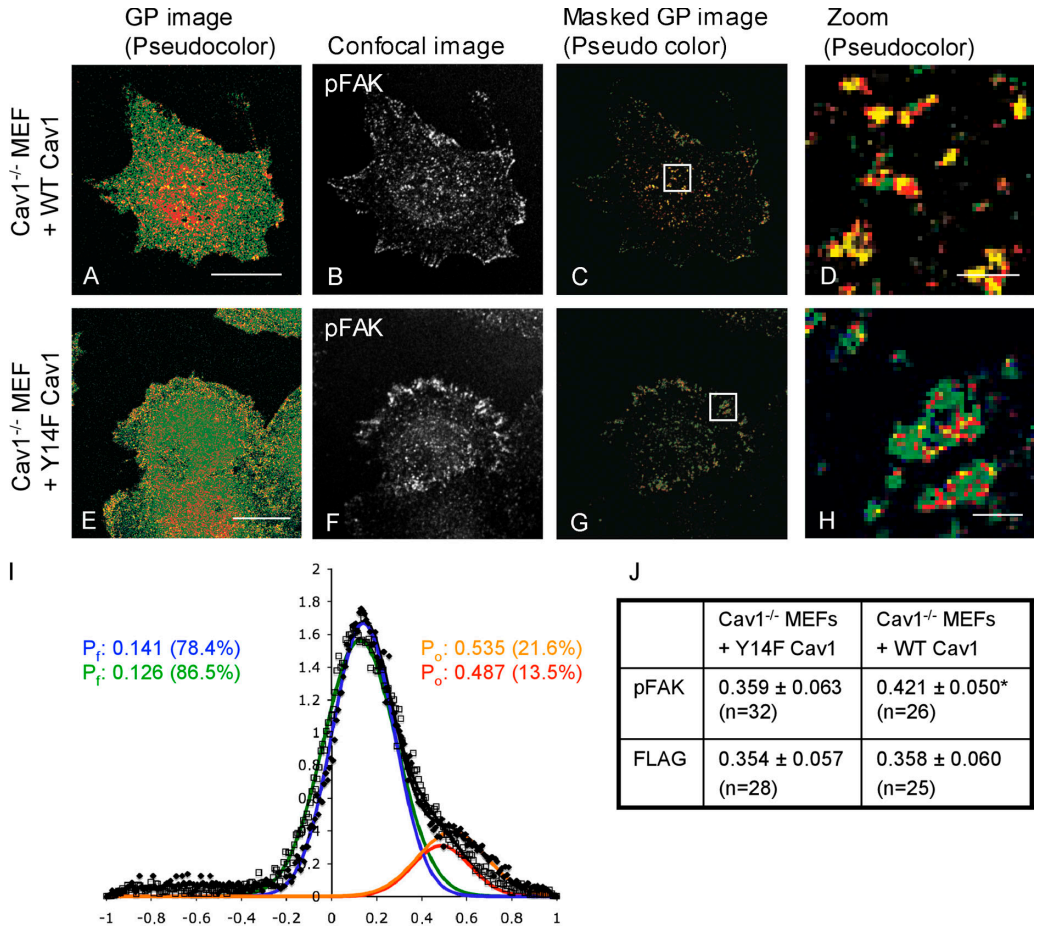

	Cav1-/- MEFs + Y14F Cav1	Cav1-/- MEFs + WT Cav1
pFAK	0.359 ± 0.063 (n=32)	0.421 ± 0.050* (n=26)
FLAG	0.354 ± 0.057 (n=28)	0.358 ± 0.060 (n=25)

Figure 5. **GP and immunofluorescent images of transfected Cav1$^{-/-}$ MEFs.** Cav1$^{-/-}$ MEFs transfected with WT Cav1 (A–D) or Y14F Cav1 (E–H) on FN-coated glass coverslips for 3 h were labeled, fixed, and immunostained as described in Materials and methods. GP images were pseudocolored (A and E) and masked as for Fig. 1. B and F show the corresponding confocal images of pFAK, C and G show the GP values of pFAK-stained regions, and D and H show magnified regions of the masked images. (I) GP distribution (closed diamonds, WT Cav1; open squares, Y14F Cav1) of transfected Cav1$^{-/-}$ MEFs (n = 20) fitted to two Gaussian populations (solid black lines). The vertical lines denote the center for fluid populations (P_f: WT Cav1, blue; Y14F Cav1, green) and ordered populations (P_o: WT Cav1, orange; Y14F Cav1, red). Centers and coverages are given for both populations. ERFs for WT- and Y14F-transfected cells were 0.0051 and 0.0036, respectively. (J) Table listing the mean ± the SD of GP values of pixels stained for pFAK or FLAG. A statistically significant difference within pFAK domains between cells transfected with WT Cav1 and Y14F Cav1 of $P < 0.001$ is indicated with an asterisk.

(21.6% vs. 13.5% for WT vs. Y14F Cav1, respectively). WT Cav1 was particularly more effective at increasing GP values within focal adhesions (marked by pFAK; GP = 0.421 ± 0.050), relative to Y14F Cav1 (GP = 0.359 ± 0.063; Fig. 5 J). The more ordered state within pFAK-positive pixels in WT Cav1–expressing cells is also visible in Fig. 5 D compared with Fig. 5 H, which shows GP values in pFAK-stained areas in Y14F Cav1–expressing cells. Thus, phosphorylation of Cav1 on Tyr14 is important for the highly ordered state of focal adhesion membranes.

To address whether the difference in GP distribution between WT Cav1– and Y14F Cav1–expressing cells can be attributed entirely to higher membrane order within focal adhesions, we analyzed pFAK-negative pixels in both cell types (unpublished data). We found no difference in membrane order outside of focal adhesions. GP in pFAK-negative areas were 0.297 ± 0.073 (n = 12) and 0.309 ± 0.096 (n = 12) for Cav1$^{-/-}$ cells transfected with WT Cav1 or Y14F Cav1, respectively. GP values outside focal adhesions in WT Cav1– or Y14F Cav1–expressing cells were significantly higher than those found in Cav1$^{-/-}$ cells (0.237 ± 0.052; n = 12), but not WT cells (0.328 ± 0.076; n = 12). It is likely that the presence of caveolae account for the difference in membrane order between Cav1$^{-/-}$ and WT cells, whereas the difference in membrane order between WT Cav1– and Y14F Cav1–expressing cells appears to be caused by the change in focal adhesions.

Cav1-dependent effects

Detachment of cells from the substratum induces internalization of raft components in WT, but not Cav1$^{-/-}$, cells (del Pozo et al., 2005). However, detachment could also perturb domains through other mechanisms. Therefore, we examined WT and Cav1$^{-/-}$ MEFs at various times after detachment (Fig. 6). Table II shows mean GP values of CTxB-positive pixels. As in PAEC, the mean GP value of GM1-positive domains slightly decreased immediately after detachment in both cell types. However, in WT cells, mean GP values continued to decrease as in PAEC. In contrast, Cav1$^{-/-}$ MEFs showed no further decrease in GP within CtxB-positive regions. When we defined plasma membrane

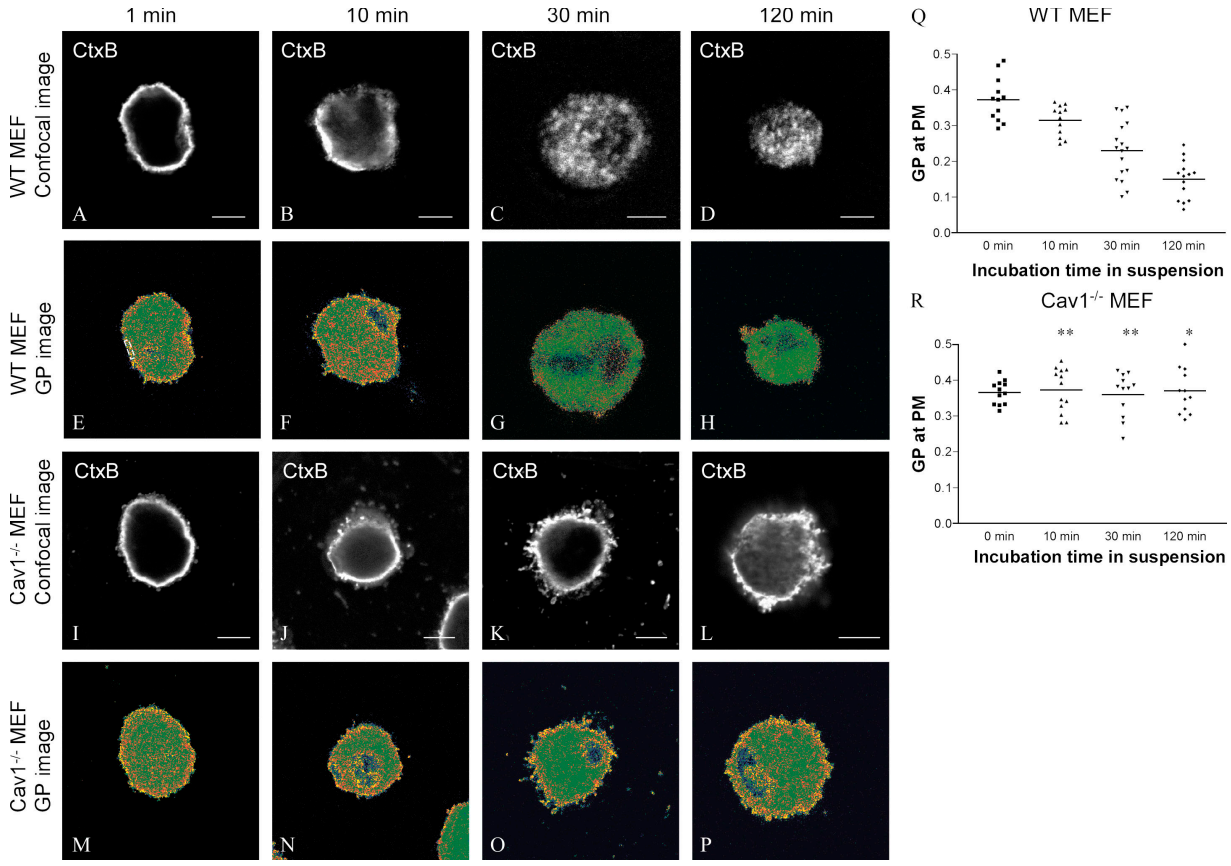

Figure 6. **GP in CtxB-stained regions in suspended WT and Cav1$^{-/-}$ MEFs.** WT MEFs (A–H and Q) and Cav1$^{-/-}$ MEFs (I–P and R) were labeled with CTxB, detached, and held in suspension for the indicated times, and processed as described in Materials and methods. A–D and I–L show confocal cross sections of the CTxB staining. E–H and M–P are pseudocolored GP images. (Q and R) GP values of the plasma membrane defined as the outer 0.5–1.2 μm of GP images (E). GP values were determined at four sites for each image, and each symbol represents the mean GP value of one image; means of means are indicated by horizontal bars. One and two asterisks in R indicate a statistical difference between WT and Cav1$^{-/-}$ MEFs of $P < 0.05$ and $P < 0.001$, respectively.

as the outer 0.5–1.2 μm (~3–6 pixels) of Laurdan-stained cells and internalized membranes as those inside this zone (indicated in Fig. 6 E), the outer regions became increasingly fluid in WT, but not Cav1$^{-/-}$, MEFs (Fig. 6, Q and R). The internalized membranes also became more fluid in WT cells. These data therefore support the hypothesis that the time-dependent decrease in fluidity of both the plasma membrane and internalized membranes after detachment are dependent on caveolin.

Discussion

Whether lipid rafts are preexisting structures in cell membranes that are determined by the self-organization of cholesterol and membrane lipids or are induced by clustering of membrane components has been a controversial question. We demonstrate that membrane order in cells, as detected by the reporter molecule Laurdan, is highly sensitive to integrin clustering and the presence and phosphorylation of caveolin. These data therefore indicate that a significant portion of the raft structure is protein dependent.

That ordered membranes at focal adhesions partially depend on the expression of Cav1 and its phosphorylation on Tyr14 suggests that localization of pYCav1 to focal adhesions recruits membrane components that induce order. Cholesterol may be one such component, which is consistent with the effects of cholesterol depletion observed here and the known binding of cholesterol by caveolin (Razani et al., 2002). Some of the order within focal adhesions is independent of Cav1 and most likely depends on integrin clustering. This idea is supported by the results that focal adhesions in Cav1$^{-/-}$ cells are still more ordered than surrounding regions, and that cell detachment decreases total order at early times before endocytosis of GM1. It also fits well with the association between activated integrins and lipid rafts (Leitinger and Hogg, 2002). These results suggest that the clustering of integrins and of pYCav1 both contribute to the assembly of membrane components into domains that are more ordered than in the unclustered state.

Consistent with the finding that cell detachment from the ECM triggers internalization of membrane domains in a caveolin-dependent manner (del Pozo et al., 2005), the fluidity of the plasma membrane showed a time-dependent decrease after detachment in WT, but not Cav1$^{-/-}$, cells. Interestingly, CTxB-stained domains became more fluid after endocytosis, suggesting that they mix with other membrane components during trafficking and lose their ordered state. The mechanisms that govern these events will have to await further characterization of the

trafficking pathways for these domains; however, the new data clearly confirm previous results based on solubility and localization of lipid raft markers.

The physical properties of membranes can have major effects on cell functions (Simons and Vaz, 2004). Ordered membrane domains may affect focal adhesion signaling through multiple mechanisms. These domains are believed to localize signaling components, including Src family kinases, H-Ras, heterotrimeric G proteins, and activated Rho family GTPases (Foster et al., 2003; del Pozo et al., 2004) and may concentrate phosphoinositides (Liu et al., 1998), which recruit or regulate focal adhesion proteins including α-actinin, vinculin, and talin (Sechi and Wehland, 2000). Ordered membrane domains may also generate an environment that localizes kinases and excludes phosphatases (Harder and Simons, 1999), and that can affect kinase activities directly by altering the configuration of membrane-associated proteins (Kalvodova et al., 2005). Although the mechanism has not been elucidated, Cav1 has been reported to modulate integrin function in several systems (Wary et al., 1998; Wei et al., 1999; del Pozo et al., 2005). The extent to which changes in local membrane composition and physical state within focal adhesions contribute to these effects will be an interesting area of future work. However, to distinguish between the direct effects of caveolin via protein–protein interactions and those caused by changes in membrane order, more tools need to be developed to specifically manipulate membrane order at focal adhesions.

Although it is functionally important, how membrane domains are targeted to or formed at specific sites within the plasma membrane is poorly understood. The lipid raft hypothesis suggests that small, highly mobile domains are formed by the self-assembly of cholesterol and sphingolipids (Simons and Ikonen, 1997; Simons and Toomre, 2000). For glycosylphosphatidylinositol–anchored (Sharma et al., 2004) or palmitoylated proteins (Plowman et al., 2005), these domains are 5–10 nm in diameter; hence, clustering, possibly by actin-dependent mechanisms (Plowman et al., 2005), is required for detection by light microscopy. The "picket fence" model proposes that nanoscale rafts are trapped in areas with a high density of transmembrane proteins and intra- and/or extracellular anchors to the membrane (Kusumi et al., 2004). We have recently shown that T cell activation sites are areas of condensed membranes (Gaus et al., 2005a), although the T cell receptor complexes are assembled by protein–protein interactions (Douglass and Vale, 2005). Hence, large multimolecular protein complexes consisting of an extracellular anchor, transmembrane proteins, and a link to the actin cytoskeleton can exert an "ordering" effect on the lipid bilayer (Gaus et al., 2005a). A similar scenario could be envisaged for focal adhesions, where the substratum and the actin cytoskeleton are linked across the lipid bilayer by integrins. This idea is consistent with our data, which demonstrate that loss of anchorage affects membrane structure quite rapidly. Within multimolecular complexes, a particular subset of proteins, such as dually palmitoylated LAT (linker for T cell activation) or caveolins, may facilitate interactions between protein complexes and raft lipids, creating a characteristic membrane structure. To what extent the recruitment of small, submicroscopic rafts contribute to the ordered membrane structure at specific sites remains to be seen. It is likely that both lipids and proteins cooperate to establish and maintain ordered membrane domains at focal adhesions.

Materials and methods

Cells and reagents

Pig aortic endothelial cells (PAEC; Cell Application, Inc.) were cultured in M199 containing 20% (vol/vol) FBS and 0.1 mg/ml heparin at 37°C in 5% CO_2. MEFs were prepared from 13.5-d-postcoitus embryos obtained by homozygous crossings of cav-1 KO or WT mice (Drab et al., 2001). MEFs cells were immortalized by continuous passage until growth rates in culture resumed the rapid rates seen in early passage MEFs. MEFs were cultured in DME supplemented with 10% (vol/vol) FBS, 2 mM L-glutamine, 100 units/L penicillin, and 100 μg/L streptomycin at 37°C in 5% CO_2. Antibodies against Cav1, pYCav1, and FAK were all obtained from BD Biosciences. Anti–phosphorylated FAK pY397 (pFAK) was purchased from Biosource, and anti-Flag M2 antibody was purchased from Sigma-Aldrich. Secondary donkey anti–rabbit or donkey anti–mouse IgG conjugated to either Cy3 or Cy5 were obtained from Jackson ImmunoResearch Laboratories. CTxB conjugated to Alexa Fluor 555 was obtained from Invitrogen. The antitubulin hybridoma E7 developed by Michael Klymkowsky was obtained from the Developmental Studies Hybridoma Bank at the University of Iowa.

Tissue culture for microscopy

Confluent cells were serum starved (0.2% FBS) overnight, and labeled with 5 μM Laurdan (6-dodecanoyl-2-dimethylaminonaphtalene; Invitrogen) in media with 0.2% FBS for 30–60 min at 37°C (Gaus et al., 2003), followed by replating on fibronectin-coated (10 μg/ml) coverslips for 1–4 h in 10–20% FBS. To deplete cholesterol, cells were incubated with 10 mM mβCD for 1 h in starvation media. Where indicated, cholesterol-depleted cells were additionally incubated with 15 μg/ml cholesterol complexed to 0.37 mM mβCD for 1 h at 37°C. Adherent cells were washed twice in warm PBS and fixed in 4% paraformaldehyde (Sigma-Aldrich) at RT for 20 min. For suspension studies, cells were detached with 0.05% EDTA-trypsin, which was stopped by addition of 0.25 mg/ml soybean trypsin inhibitor (Sigma-Aldrich). Cells were sedimented, resuspended in medium containing 10 mg/ml BSA (Sigma-Aldrich; del Pozo et al., 2002), and incubated for the indicated times; they were then fixed in 4% paraformaldehyde (for 20 min at RT), cytospun onto poly-L-lysine–coated (Sigma-Aldrich) coverslips (for 5 min at 950 RPM), and fixed again in 4% paraformaldehyde (for 20 min at RT). To stain for GM1, live cells on ice were incubated with 0.1 mg/ml CTxB–Alexa Fluor 555 for 10–15 min, washed, and fixed. MEFs were transfected with plasmids encoding either FLAG-tagged WT Cav1 or Y14F Cav1 using MEF2 solution combined with the T20 program of the Amaxa system. Transfections with empty vectors were used as controls. Successfully transfected cells were identified by immunostaining with anti-FLAG antibodies.

For immunofluorescence, fixed cells were blocked with 5% normal donkey serum (Jackson ImmunoResearch Laboratories) in 0.1% saponin (Sigma-Aldrich) and immunolabeled for 1 h each with primary and secondary antibodies, washed after each incubation period, and mounted with mounting media containing antifading agents (ProSciTech).

Microscopy

Images were obtained with a microscope (DM IRE2; Leica) equipped with photon-multiplier tubes and acquisition software (Leica). Laurdan fluorescence was excited at 800 nm with a multiphoton laser system (Verdi/Mira 900; Coherent). Laurdan intensity images were recorded simultaneously and emissions were in the range of 400–460 and 470–530 nm (Gaus et al., 2003). Microscopy calibrations were performed as described previously (Gaus et al., 2003). For confocal microscopy a helium-neon laser was used to excite Cy3 (Ex: 543 nm; Em: 550–620 nm) and Cy5 (Ex: 633 nm; Em 650–720 nm) with appropriate cut-off filters and pinhole widths. For fixed cells, a 100× oil objective, NA 1.4, was used; for live cell, a 63× water objective, NA 1.3, was used, and images were recorded at RT.

Image analysis

The GP, which is defined as

$$GP = \frac{I_{(400-460)} - I_{(470-530)}}{I_{(400-460)} + I_{(470-530)}},$$

was calculated for each pixel in the two Laurdan intensity images using software from WiT (Gaus et al., 2003). The custom-made WiT algorithm converts the intensity images into floating point format, calculates the GP value for each pixel, and converts the image back to an 8-bit unsigned format. To set background values to zero, the denominator ($I_{(400-460)} + I_{(470+530)}$) is converted to a binary image with background values set to zero, nonbackground values set to one, and the binary image multiplied with the GP image. Final GP images were pseudocolored in Photoshop (Adobe). GP distributions were obtained from the histograms of the GP images, normalized (sum = 100), and fitted to two Gaussian distributions using the nonlinear fitting algorithm using Excel software (Microsoft). The quality of the fit was determined by the ERF, as follows:

$$\mathrm{ERF} = \frac{\sum_i \left[y(i)_{obs} - y(i)_{fit}\right]^2}{\sum_i y(i)_{obs}^2},$$

where $y(i)_{obs}$ and $y(i)_{fit}$ are the experimental and calculated values, respectively. A fit is regarded as excellent when the ERF < 0.01 (Gaus et al., 2001).

To determine GP values at focal adhesions, background-corrected confocal images were used to mask the GP images; the confocal images defined the regions of interest and the mean GP value of the regions of interest was determined for each image. GP values were corrected using the G-factor obtained for Laurdan in DMSO for each experiment (Gaus et al., 2003).

Statistics

The means and SD of two populations were compared with unpaired *t* tests, assuming unequal variances. For multiple comparisons, one-way analysis of variance with Tukey's posttesting was performed, assuming Gaussian distributions (Prism; GraphPad Software, Inc.).

Online supplemental material

Fig. S1 shows Laurdan microscopy. Fig. S2 shows cholesterol depletion. Fig. S3 shows integrin activation. Table S1 shows GP values of mock-transfected MEFs. Online supplemental material is available at http://www.jcb.org/cgi/content/full/jcb.200603034/DC1.

K. Gaus acknowledges support for this work from the Australian Research Council, the National Health and Medical Research Council, and the Australian National Heart Foundation. M.A. Schwartz was supported by United States Public Health Service grant RO1 GM47214.

Submitted: 7 March 2006
Accepted: 25 July 2006

References

Bagatolli, L.A., S.A. Sanchez, T. Hazlett, and E. Gratton. 2003. Giant vesicles, Laurdan, and two-photon fluorescence microscopy: evidence of lipid lateral separation in bilayers. *Methods Enzymol.* 360:481–500.

Brown, D.A., and E. London. 1998. Structure and origin of ordered lipid domains in biological membranes. *J. Membr. Biol.* 164:103–114.

Chapman, H.A., Y. Wei, D.I. Simon, and D.A. Waltz. 1999. Role of urokinase receptor and caveolin in regulation of integrin signaling. *Thromb. Haemost.* 82:291–297.

Decker, L., and C. Ffrench-Constant. 2004. Lipid rafts and integrin activation regulate oligodendrocyte survival. *J. Neurosci.* 24:3816–3825.

del Pozo, M.A., W.B. Kiosses, N.B. Alderson, N. Meller, K.M. Hahn, and M.A. Schwartz. 2002. Integrins regulate GTP-Rac localized effector interactions through dissociation of Rho-GDI. *Nat. Cell Biol.* 4:232–239.

del Pozo, M.A., N.B. Alderson, W.B. Kiosses, H.H. Chiang, R.G. Anderson, and M.A. Schwartz. 2004. Integrins regulate Rac targeting by internalization of membrane domains. *Science*. 303:839–842.

del Pozo, M.A., N. Balasubramanian, N.B. Alderson, W.B. Kiosses, A. Grande-Garcia, R.G. Anderson, and M.A. Schwartz. 2005. Phospho-caveolin-1 mediates integrin-regulated membrane domain internalization. *Nat. Cell Biol.* 7:901–908.

Douglass, A.D., and R.D. Vale. 2005. Single-molecule microscopy reveals plasma membrane microdomains created by protein-protein networks that exclude or trap signaling molecules in T cells. *Cell*. 121:937–950.

Drab, M., P. Verkade, M. Elger, M. Kasper, M. Lohn, B. Lauterbach, J. Menne, C. Lindschau, F. Mende, F.C. Luft, et al. 2001. Loss of caveolae, vascular dysfunction, and pulmonary defects in caveolin-1 gene-disrupted mice. *Science*. 293:2449–2452.

Faull, R.J., N.L. Kovach, J.M. Harlan, and M.H. Ginsberg. 1993. Affinity modulation of integrin α5β1: regulation of the functional response by soluble fibronectin. *J. Cell Biol.* 121:155–162.

Foster, L.J., C.L. De Hoog, and M. Mann. 2003. Unbiased quantitative proteomics of lipid rafts reveals high specificity for signaling factors. *Proc. Natl. Acad. Sci. USA*. 100:5813–5818.

Fra, A.M., E. Williamson, K. Simons, and R.G. Parton. 1994. Detergent-insoluble glycolipid microdomains in lymphocytes in the absence of caveolae. *J. Biol. Chem.* 269:30745–30748.

Frank, P.G., M.W. Cheung, S. Pavlides, G. Llaverias, D.S. Park, and M.P. Lisanti. 2006. Caveolin-1 and the regulation of cellular cholesterol homeostasis. *Am. J. Physiol. Heart Circ. Physiol.* 291:H677–H686.

Gaus, K., J.J. Gooding, R.T. Dean, L. Kritharides, and W. Jessup. 2001. A kinetic model to evaluate cholesterol efflux from THP-1 macrophages to apolipoprotein A-1. *Biochemistry*. 40:9363–9373.

Gaus , K., E. Gratton, E.P. Kable, A.S. Jones, I. Gelissen, L. Kritharides, and W. Jessup. 2003. Visualizing lipid structure and raft domains in living cells with two-photon microscopy. *Proc. Natl. Acad. Sci. USA*. 100:15554–15559.

Gaus, K., E. Chklovskaia, B. Fazekas de St Groth, W. Jessup, and T. Harder. 2005a. Condensation of the plasma membrane at the site of T lymphocyte activation. *J. Cell Biol.* 171:121–131.

Gaus, K., M. Rodriguez, K.R. Ruberu, I. Gelissen, T.M. Sloane, L. Kritharides, and W. Jessup. 2005b. Domain-specific lipid distribution in macrophage plasma membranes. *J. Lipid Res.* 46:1526–1538.

Gaus, K., T. Zech, and T. Harder. 2006. Visualizing membrane microdomains by Laurdan 2-photon microscopy. *Mol Membr. Biol*. 23:41–48.

Harder, T., and K. Simons. 1999. Clusters of glycolipid and glycosylphosphatidylinositol-anchored proteins in lymphoid cells: accumulation of actin regulated by local tyrosine phosphorylation. *Eur. J. Immunol.* 29:556–562.

Harder, T., P. Scheiffele, P. Verkade, and K. Simons. 1998. Lipid domain structure of the plasma membrane revealed by patching of membrane components. *J. Cell Biol.* 141:929–942.

Harris, T.J., and C.H. Siu. 2002. Reciprocal raft-receptor interactions and the assembly of adhesion complexes. *Bioessays*. 24:996–1003.

Heerklotz, H., H. Szadkowska, T. Anderson, and J. Seelig. 2003. The sensitivity of lipid domains to small perturbations demonstrated by the effect of Triton. *J. Mol. Biol.* 329:793–799.

Horton, J.D. 2002. Sterol regulatory element-binding proteins: transcriptional activators of lipid synthesis. *Biochem. Soc. Trans.* 30:1091–1095.

Hynes, R.O. 2002. Integrins: bidirectional, allosteric signaling machines. *Cell*. 110:673–687.

Kalvodova, L., N. Kahya, P. Schwille, R. Ehehalt, P. Verkade, D. Drechsel, and K. Simons. 2005. Lipids as modulators of proteolytic activity of BACE: involvement of cholesterol, glycosphingolipids, and anionic phospholipids in vitro. *J. Biol. Chem.* 280:36815–36823.

Kindzelskii, A.L., R.G. Sitrin, and H.R. Petty. 2004. Cutting edge: optical microspectrophotometry supports the existence of gel phase lipid rafts at the lamellipodium of neutrophils: apparent role in calcium signaling. *J. Immunol.* 172:4681–4685.

Kusumi, A., I. Koyama-Honda, and K. Suzuki. 2004. Molecular dynamics and interactions for creation of stimulation-induced stabilized rafts from small unstable steady-state rafts. *Traffic*. 5:213–230.

Leitinger, B., and N. Hogg. 2002. The involvement of lipid rafts in the regulation of integrin function. *J. Cell Sci.* 115:963–972.

Liu, Y., L. Casey, and L.J. Pike. 1998. Compartmentalization of phosphatidylinositol 4,5-bisphosphate in low-density membrane domains in the absence of caveolin. *Biochem. Biophys. Res. Commun.* 245:684–690.

Munro, S. 2003. Lipid rafts: elusive or illusive? *Cell*. 115:377–388.

Pampori, N., T. Hato, D.G. Stupack, S. Aidoudi, D.A. Cheresh, G.R. Nemerow, and S.J. Shattil. 1999. Mechanisms and consequences of affinity modulation of integrin alpha(V)beta(3) detected with a novel patch-engineered monovalent ligand. *J. Biol. Chem.* 274:21609–21616.

Pelkmans, L., and A. Helenius. 2002. Endocytosis via caveolae. *Traffic*. 3:311–320.

Pelkmans, L., and M. Zerial. 2005. Kinase-regulated quantal assemblies and kiss-and-run recycling of caveolae. *Nature*. 436:128–133.

Pelkmans, L., D. Puntener, and A. Helenius. 2002. Local actin polymerization and dynamin recruitment in SV40-induced internalization of caveolae. *Science*. 296:535–539.

Plowman, S.J., C. Muncke, R.G. Parton, and J.F. Hancock. 2005. H-ras, K-ras, and inner plasma membrane raft proteins operate in nanoclusters with differential dependence on the actin cytoskeleton. *Proc. Natl. Acad. Sci. USA*. 102:15500–15505.

Porter, J.C., and N. Hogg. 1998. Integrins take partners: cross-talk between integrins and other membrane receptors. *Trends Cell Biol.* 8:390–396.

Razani, B., S.E. Woodman, and M.P. Lisanti. 2002. Caveolae: from cell biology to animal physiology. *Pharmacol. Rev.* 54:431–467.

Scherer, P.E., R.Y. Lewis, D. Volonte, J.A. Engelman, F. Galbiati, J. Couet, D.S. Kohtz, E. van Donselaar, P. Peters, and M.P. Lisanti. 1997. Cell-type and tissue-specific expression of caveolin-2. Caveolins 1 and 2 co-localize and form a stable hetero-oligomeric complex in vivo. *J. Biol. Chem.* 272:29337–29346.

Schwartz, M.A. 1997. Integrins, oncogenes, and anchorage independence. *J. Cell Biol.* 139:575–578.

Schwartz, M.A. 2001. Integrin signaling revisited. *Trends Cell Biol.* 11:466–470.

Sechi, A.S., and J. Wehland. 2000. The actin cytoskeleton and plasma membrane connection: PtdIns(4,5)P(2) influences cytoskeletal protein activity at the plasma membrane. *J. Cell Sci.* 113:3685–3695.

Sharma, P., R. Varma, R.C. Sarasij, Ira, K. Gousset, G. Krishnamoorthy, M. Rao, and S. Mayor. 2004. Nanoscale organization of multiple GPI-anchored proteins in living cell membranes. *Cell*. 116:577–589.

Simons, K., and E. Ikonen. 1997. Functional rafts in cell membranes. *Nature*. 387:569–572.

Simons, K., and D. Toomre. 2000. Lipid rafts and signal transduction. *Nat. Rev. Mol. Cell Biol.* 1:31–39.

Simons, K., and W.L. Vaz. 2004. Model systems, lipid rafts, and cell membranes. *Annu. Rev. Biophys. Biomol. Struct.* 33:269–295.

Varma, R., and S. Mayor. 1998. GPI-anchored proteins are organized in sub-micron domains at the cell surface. *Nature*. 394:798–801.

Wary, K.K., A. Mariotti, C. Zurzolo, and F.G. Giancotti. 1998. A requirement for caveolin-1 and associated kinase Fyn in integrin signaling and anchorage-dependent cell growth. *Cell*. 94:625–634.

Wei, Y., X. Yang, Q. Liu, J.A. Wilkins, and H.A. Chapman. 1999. A role for caveolin and the urokinase receptor in integrin-mediated adhesion and signaling. *J. Cell Biol.* 144:1285–1294.

Zacharias, D.A., J.D. Violin, A.C. Newton, and R.Y. Tsien. 2002. Partitioning of lipid-modified monomeric GFPs into membrane microdomains of live cells. *Science*. 296:913–916.